J. Mater. Chem. C, DOI: 10.1039/c7tc03721j

Sub-second photonic processing of solution-deposited single layer and heterojunction metal oxide thin-film transistors using a high-power xenon flash lamp

Received 00th January 20xx,
Accepted 00th January 20xx

DOI: 10.1039/x0xx00000x

www.rsc.org/

Kornelius Tetzner,[*a] Yen-Hung Lin,[a] Anna Regoutz,[b] Akmaral Seitkhan,[c] David J. Payne[b] and Thomas D. Anthopoulos[*a, c]

We report the fabrication of solution-processed In_2O_3 and In_2O_3/ZnO heterojunction thin-film transistors (TFTs) where the precursor materials were converted to their semiconducting state using high power light pulses generated by a xenon flash lamp. In_2O_3 TFTs prepared on glass substrates exhibited low-voltage operation (≤2 V) and high electron mobility of ~6 cm^2/Vs. By replacing the In_2O_3 layer with a photonically processed In_2O_3/ZnO heterojunction, we were able to increase the electron mobility to 36 cm^2/Vs, while maintaining the low-voltage operation. Although the level of performance achieved in these devices is comparable to control TFTs fabricated via thermal annealing at 250 °C for 1 h, the photonic treatment approach adopted here is extremely rapid with a processing time of less than 18 s per layer. With the aid of a numerical model we were able to analyse the temperature profile within the metal oxide layer(s) upon flashing revealing a remarkable increase of the layer's surface temperature to ~1000 °C within ~1 ms. Despite this, the backside of the glass substrate remains unchanged and close to room temperature. Our results highlights the applicability of the method for the facile manufacturing of high performance metal oxide transistors on inexpensive large-area substrates.

Introduction

Metal oxide semiconductors such as ZnO, In_2O_3, Ga_2O_3 or SnO_2 have drawn great attention in recent years due to their excellent optical and electrical properties including high optical transparency and charge carrier mobility, as well as reliable and uniform device-to-device performance. This unique combination of highly attractive characteristics makes the family of metal oxides an attractive alternative to incumbent Si-based technologies for applications in electronic devices such as thin-film transistors (TFTs).[1-3] Furthermore, the relatively simple chemistry of most metal oxides makes them compatible with solution-based processing routes, and hence low-cost, large-volume manufacturing.[4] That is why in recent years oxide semiconductors have successfully been utilized across a spectrum of applications including displays,[5] biosensors,[6] and radio-frequency identification tags[7] that can be manufactured using different solution-based processing techniques amongst which printing[8] and spraying[9].

Despite the numerous advantages, however, the vast majority of high performance solution-processable metal oxides rely on high temperature thermal annealing (typically >200 °C) for prolonged periods of time (>1h).[10] This makes device/system processing lengthy whilst limits the choice of substrate materials to those able to cope with such high temperatures. To overcome this issue, significant effort has been focussing on the use of optical sintering techniques using lasers[11] as well as high power xenon flash lamps as an alternative to thermal annealing.[12-16] In spite the promising results, however, most of the work has been restricted to Si substrates and neither glass nor plastic have been explored, possibly due to their unfavourable optical properties. In particular, unlike Si the high optical transparency of glass and plastic in the spectral range of the xenon flash lamp impedes the generation of sufficient thermal energy due to low absorption in order to chemically convert the oxide precursor material to its semiconducting state.[17] Therefore, development of alternative approaches that enable the utilization of inexpensive and mechanically flexible substrate materials is critical for the successful utilization of the technology in the emerging sector of printed, large-area electronics.

Here we report the rapid fabrication of high-performance metal oxide TFTs on glass via photonic processing, while identifying the various fabrication boundaries related to the

[a] Department of Physics and Centre for Plastic Electronics, Blackett Laboratory, Imperial College London, London SW7 2BW, United Kingdom
E-Mail: k.tetzner@imperial.ac.uk
[b] Department of Materials, London Royal School of Mines, Imperial College London, London SW7 2AZ, United Kingdom
[c] Division of Physical Sciences and Engineering, King Abdullah University of Science and Technology, Thuwal 23955-6900, Saudi Arabia
E-Mail: thomas.anthopoulos@kaust.edu.sa

† Footnotes relating to the title and/or authors should appear here.
Electronic Supplementary Information (ESI) available: [details of any supplementary information available should be included here]. See DOI: 10.1039/x0xx00000x

material stack composition and processing parameters such as light-pulse intensity and duration when used in conjunction with optically transparent substrates. In particular, we demonstrate the applicability of the method for the growth of low-dimensional In_2O_3 as well as In_2O_3/ZnO heterojunctions and their application in high performance TFTs. In the case of photonically-processed In_2O_3 devices, a maximum electron mobility value of ≈6 cm^2/Vs is obtained, whilst for In_2O_3/ZnO heterojunction devices this value reaches 36 cm^2/Vs. The exceptional performance achieved in the heterojunction TFTs is attributed to the formation of a quasi-two-dimensional electron gas (2DEG)-like system at the vicinity of the In_2O_3/ZnO heterointerface.[10,18,19] By combining heterojunction channels with solution-processed bilayer high-k dielectrics consisting of aluminium oxide (AlO_X) and zirconium oxide (ZrOx), we are also able to reduce the operating voltage of the transistors to ≤2 V. In addition to the remarkable performance, the photonic process adopted here is rapid with overall treatment time per layer of <18 sec. Finally, the elemental composition, electronic and microstructural properties of best performing metal oxide systems and devices are investigated by means of atomic force microscopy (AFM), X-ray photoelectron spectroscopy (XPS), high resolution transmission electron microscopy (HRTEM), electron energy loss spectroscopy (EELS) and energy dispersive spectroscopy (EDS).

Experimental

Preparation of metal oxide solutions

Indium oxide (In_2O_3) and zinc oxide (ZnO) precursor solutions were prepared by dissolving 30 mg/mL indium nitrate hydrate ($In(NO_3)_3{\cdot}xH_2O$, 99.99%, Indium Corporation) in 2-methoxyethanol (99.8%, Sigma-Aldrich), and 10 mg/mL ZnO (99.99%, Sigma-Aldrich) nanoparticles in aqueous ammonium hydroxide solution (NH_4OH, 50% v/v aqn. soln., Alfa Aesar) under constant stirring at room temperature. The zirconium oxide (ZrOx) precursor solution was prepared according to synthesis routes reported previously in the literature[20] by dissolving zirconium acetylacetonate ($Zr(C_5H_7O_2)_4$) (98%, Sigma-Aldrich) in N,N-dimethylformamide, or DMF (C_3H_7NO, Sigma-Aldrich), at a concentration of 0.15 M in inert gas atmosphere with the addition of an equal molar concentration of ethanolamine (MEA, C_2H_7NO) (≥ 99% Sigma-Aldrich). The solution was stirred vigorously at 90° C for 1 h.

Transistor fabrication and characterisation

Bottom-gate, top-contact TFTs were fabricated on borosilicate glass substrates that were ultrasonically cleaned in deionized water, acetone, and 2-propanol for 10 min each prior to use. Gate electrodes were deposited by evaporating 100 nm of Aluminium (Al) through a shadow mask in high vacuum (10^{-6} mbar). Following, a thin layer of native AlO_X was grown by exposing the electrodes to ozone generated by a low-pressure mercury UV lamp (5 mW/cm^2). Subsequently, the as-prepared ZrOx solution was spin-coated onto the substrates at 3000 rpm for 30 s in nitrogen followed by curing the samples with a metal halide lamp of 250 mW/cm^2 equipped with a filter of UVA spectrum, for 90 min in ambient air. Next, three layers of In_2O_3 precursor solution were sequentially spin-cast at 3000 rpm for 30 s in ambient air. After each deposition, the films were soft-baked at 130 °C for 5 min in order to remove solvent residues and subsequently subjected to the photonic treatment step(s). Heterojunction devices were realised by spin-coating an additional layer of the ZnO precursor solution on top of the photonically converted In_2O_3 layer and dried at 110 °C for 5 min. Control devices were fabricated by thermally annealing each semiconductor layer at 250 °C in air for 1 h. Transistor fabrication was completed by evaporating Al source/drain contacts through a metal shadow mask. Resulting TFTs featured channels with length (L) and width (W) of 40 µm and 1000 µm, respectively. Transistor characterisation was carried out under nitrogen atmosphere at room temperature using an Agilent B2902A parameter analyser. The field-effect mobility was extracted from the transfer characteristics in saturation regime using the gradual channel approximation model:

$$\mu_{sat} = \frac{L}{WC_i}\frac{\partial^2 I_{D(sat)}}{\partial^2 V_G^2}$$

where, I_D(sat) the channel current in saturation and C_i the geometric capacitance of the gate dielectric. The threshold voltage, V_{Th}, was extracted from the x-intercept of a linear fit to the $\sqrt{I_D}$of vs V_G plot. The onset voltage, V_{ON}, was estimated directly from the transfer characteristics.

Photonic treatment of the metal oxide semiconducting layers

The photonic treatment of the metal oxide layers was carried out using a Novacentrix Pulse Forge 1300 with radiant optical energies of 4 and 5 J/cm^2 and pulse lengths of 300 and 500 µs. The number of pulses was set to 1, 10 and 20 with a fire rate of 1.2 Hz. The samples were placed at a distance of 5 mm below the lamp window. The emission spectrum of the xenon bulb in the Pulse Forge is ranging between 200 and 1500 nm. The temperature distribution in the material stack was estimated using the simulation software SimPulse.

Material Characterisation

The surface topography of the metal oxide layers studied were investigated by AFM in intermittent contact mode using an Agilent 5500AFM system.

XPS spectra were recorded on a Thermo Scientific K-Alpha+ X-ray photoelectron spectrometer operating at $2x10^{-9}$ mbar base pressure. This system incorporates a monochromated, microfocused Al Kα X-ray source (hν = 1486.6 eV) and a 180° double focusing hemispherical analyser with a 2D detector. The X-ray source was operated at 6 mA emission current and 12 kV anode bias. Data were collected at 200 eV pass energy for survey, 20 eV pass energy for core level, and 15 eV pass energy for valence band spectra using an X-ray spot size of 400 μm^2. A flood gun was used to minimize sample charging. All data were analysed using the Avantage software package.

For HRTEM, EELS and EDS analyses the samples were prepared with a focused ion beam (FIB) in a scanning electron microscope (Helios 400s, FEI) equipped with a nanomanipulator (Omniprobe, AutoProbe300). Sequential carbon and platinum layers were deposited under the electron beam assistance to protect the sample surface from the ion beam during the later stages of the sample preparation. Ga ion beam (30kV, 9nA) was employed to mill and cut the sample from the bulk and then attach it to a copper grid according to a lift-out method. After that the sample was thinned down with the ion-beam assistance (30kV, 93pA) to finally reach the thickness of ca. 50-70 nm. The sample was cleaned with the ion beam (2kV, 28pA) to remove the damaged areas and other contamination.

The cross-sectional HRTEM images were acquired with a transmission electron microscope (Titan 80-300, FEI) at 300kV operating voltage. The chemical composition of the samples was analysed with the Energy Dispersive X-Ray Spectrometer of the aforementioned microscope. The EELS maps were acquired in a scanning TEM (STEM) mode with the help of Gatan Imaging Filter (GIF) Qunatum 966.

Results and Discussion

The photonically-induced conversion process relies on the absorption of light and its subsequent transformation to thermal energy, which in turn initiates the chemical reaction/conversion of the deposited precursor materials(s) located on the substrate.[17,21] In order to minimise the thermal load on the substrate, especially when temperature-sensitive materials such as plastics are in use, the optical energy should be absorbed within the shortest possible time and preferably by the precursor layer(s) and not by the substrate so that a thermal gradient in between the two is established. A major requirement to reach this non-equilibrium condition is the use of substrates that do not readily absorb light such as glass or plastics. In the case of Si the light energy is absorbed primarily by the substrate itself heating up the whole material stack so that no thermal gradient exists. For the latter, the temperature of the Si substrate is nearly identical to that of the thin-film (see ESI,† **Fig. S1**). In addition, due to the high thermal conductivity of Si high radiant powers and/or number of flash pulses are needed to reach temperatures suitable for the metal oxide precursor conversion[22].

Applying the photonic curing process to solution-processed metal oxides deposited on glass or plastic substrates reveals the issue that the absorption of light is drastically impeded due to the high transparency of all materials, including that of the oxide(s). Here the introduction of an additional light absorbing layer where heat can be generated, becomes necessary. Recently, it was shown that thin metal layers deposited by evaporation are capable of absorbing enough light and heat up sol-gel derived hafnium oxide layers deposited on the top of these layers.[23] Comparative studies using the software SimPulse reveal that metals such as platinum, titanium or chromium show the highest thermal response on borosilicate glass substrates due to their high absorbance within the spectral range of the xenon flash lamp between 200 and 1500 nm (see ESI,† **Fig. S2**). Interestingly, aluminium also shows reasonable thermal response due to sufficient light absorption despite its high reflectance across the entire xenon light emission spectrum.[24] Another parameter that plays an important role is the metal layer thickness which has to be considered for reaching optimum thermal response. These findings lead to the conclusion that in a bottom-gate TFT architecture the gate metallisation can in principle be exploited as the light absorbing component to heat and chemically convert the metal oxide precursor layer(s) deposited atop. Since Al is a low-cost metal and can be deposited using different techniques on a wide range of substrate materials, we opted using it as the gate metallisation with thickness of 100 nm. A combination of deep--ultraviolet (DUV)-induced native AlO_X and solution-processed ZrO_X dielectrics featuring high geometrical capacitances of ≈235 nF/cm^2, were used in order to realise low-operating voltage TFTs (see ESI,† **Fig. S3**). The use of the solution processed ZrO_X layer has also helped to smoothen the rough Al gate electrode reducing its root-mean-square (rms) surface roughness from 1.2 to 0.8 nm (see ESI,† **Fig. S4**).

In order to evaluate the optimum photonic processing conditions several solution-processed In_2O_3 TFTs were fabricated with varying light flashing parameters such as optical energy, light pulse duration and number of pulses (see ESI,† **Fig. S5**). Electrical characterisation of each sample was carried out by measuring the transfer characteristics of the resulting TFTs. This allowed rapid evaluation of the process parameters employed. The comparative study revealed that the use of pulses with energy density of 4 J/cm^2 and duration of 500 µs required a high number of pulses (>20) to be used in order to convert the precursor layer to its semiconducting state so moderate TFT performance can be obtained. On the contrary, use of pulses with energy density and duration of 5 J/cm^2 and 300 µs, respectively, revealed that exposure of the sample to even a single pulse is already enough to convert the In_2O_3 precursor layer to its semiconducting state and yield TFTs with electron mobilities of ~2 cm^2/Vs. Increasing the number of pulses to >1 was found to result to In_2O_3 layer with significantly higher electrical conductivity rendering them unsuitable for use in TFTs. By reducing the optical energy density to 4 J/cm^2, while maintaining the pulse duration to 300 µs, yielded In_2O_3 TFTs with significantly improved channel on/off current ratios of around 10^4. Unfortunately, these devices suffered from large operating hysteresis, an effect most likely attributed to incomplete conversion of the precursor to In_2O_3. The optimum pulse energy density and pulse duration were found to be 5 J/cm^2 and 500 µs, respectively, and were used for the fabrication of all TFTs that will be analysed herein.

The evolution of the transistor transfer characteristics after soft-baking the solution-processed In_2O_3 precursor layer at 130 °C for 5 min and subjecting them to 1, 10 and 20 xenon light pulses (500 µs at 5 J/cm^2) is presented in **Fig. 1(a)**, while a summary of the extracted transistor parameters is given in **Table 1**. Additional plots by calculating the square-root of the drain current are shown in ESI,† **Fig. S6**. The results reveal that devices based on the softly-baked (130 °C) In_2O_3 precursor layer do not show any transistor functionality. This is because the

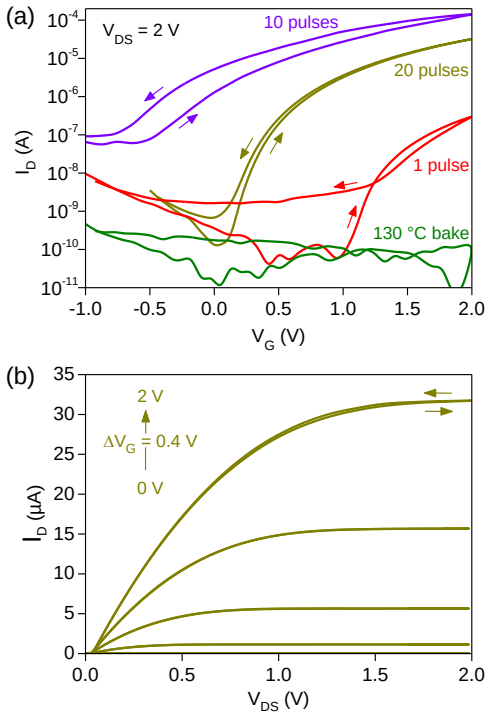

baking temperature is not sufficient to convert the precursor material to In_2O_3. Subjecting the soft-baked precursor layers to a single xenon pulse, is enough to give working n-channel TFTs with a clear gate-dependent current-voltage modulation. However, the performance of these devices was consistently low with a maximum electron mobility of ≈0.2 cm^2/Vs and an on/off channel current ratio of 10^2. By increasing the number of pulses to 10 the electron mobility of the TFTs increases and reaches a value of ~11 cm^2/Vs. The on/off current ratio also increases by one order of magnitude to ~10^3. Despite the improvement, however, the devices exhibit notable operating hysteresis a feature most likely attributed to the incomplete chemical conversion of the precursor material. The latter is known to be associated with a higher concentration of electron traps and as such dramatically affect charge transport.[25]

Subjecting the devices to a total of 20 optical pulses results in a further device improvement with the resulting In_2O_3 TFTs exhibiting on/off current ratio of ~10^5 but with a slightly reduced electron mobility value of 6 cm^2/Vs. Importantly, the transistors exhibit negligible hysteresis and an overall performance that is comparable to control In_2O_3 TFTs fabricated via conventional thermal annealing at 250 °C for 1 h in air (see ESI,† **Fig. S7(a)**). Moreover, the output characteristics (**Fig. 1(b)**) of the In_2O_3 TFTs subjected to 20 optical pulses show good saturation with negligible hysteresis and no signs of contact resistance.

Fig. 1 (a) Transfer characteristics measured for In_2O_3 TFTs after soft-baking at 130 °C and subsequently exposed to 1, 10 and 20 xenon light pulses with energy density per pulse and duration of 5 J/cm² and 500 µs, respectively. Multiple pulse exposure was performed at a fire rate of 1.2 Hz. (b) Corresponding output characteristics for the In_2O_3 TFT treated with 20 pulses.

Table 1 Electrical parameters of solution-processed In_2O_3 transistors fabricated using different post-deposition treatment conditions.

Processing conditions	μ_{sat} ($cm^2V^{-1}s^{-1}$)	V_{TH} (V)	V_{ON} (V)	On/off ratio
1 Flash (5 J/cm², 500 µs)	0.2	1.2	1	1 x 10^2
10 Flashes (5 J/cm², 500 µs)	11.3	0.3	-0.6	2 x 10^3
20 Flashes (5 J/cm², 500 µs)	6	0.6	0.1	8 x 10^4
Thermal annealing at 250 °C for 1 h	9	0.5	0.1	6 x 10^3

In an effort to improve the performance of the photonically treated TFTs, but also further exploit the potential of the method, we fabricated transistors comprising an In_2O_3/ZnO heterostructure as the electron-transporting channel. This was achieved by spin-coating the ZnO precursor material on top of the pre-converted In_2O_3 layer and soft-baked it at 110 °C in air. The bilayer was then subjected to 1, 10 and 20 light pulses using the pre-established optimal process conditions (500 µs pulse duration @ 5 J/cm²). In the case of single layer ZnO devices, the chosen photonic treatment conditions yield comparable performance to ZnO transistors prepared by thermal annealing at 250 °C for 1 h in ambient air (see ESI,† **Fig. S7(b), Fig. S9 and Table S1**). We therefore opted to use the same process parameters for the photonic treatment of In_2O_3/ZnO heterostructure devices.

Fig. 2(a) shows the transfer characteristics for a representative In_2O_3/ZnO heterostructure TFT while the key device parameters are summarized in **Table 2**. Additional plots by calculating the square-root of the drain current are shown in ESI,† **Fig. S8.** TFTs subjected to a single xenon light pulse exhibit

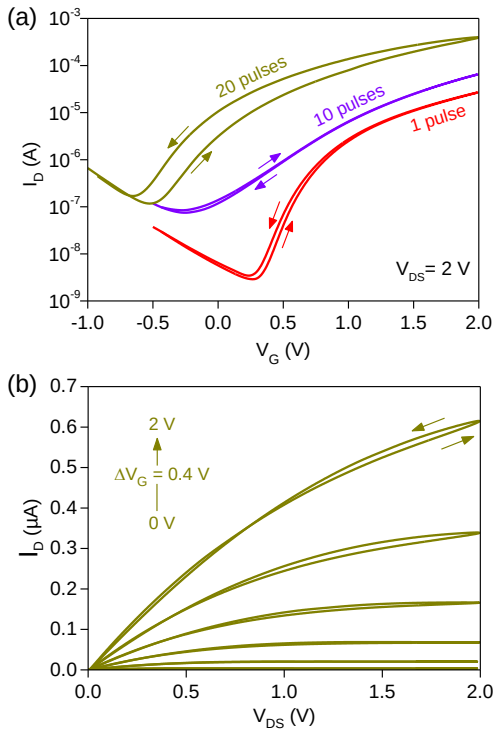

Fig. 2 (a) Transfer characteristics of heterostructure thin-film transistors consisting of photonically cured In_2O_3 films using 20 xenon pulses and single layer ZnO dried at 110 °C which were subsequently exposed to 1, 10 and 20 xenon flash pulses of energy densities of 5 J/cm² and pulse durations of 500 µs at a fire rate of 1.2 Hz and (b) corresponding output characteristics for In_2O_3/ZnO transistors flashed each layer with 20 pulses.

Table 2 Electrical parameters of solution-processed In_2O_3/ZnO transistors fabricated using different post-deposition treatment conditions. The In_2O_3 layers were photonically treated with 20 pulses (5 J/cm², 500 µs) prior to ZnO deposition.

Processing conditions	μ_{sat} ($cm^2V^{-1}s^{-1}$)	V_{TH} (V)	V_{ON} (V)	On/off ratio
1 Flash (5 J/cm², 500 µs)	4.7	0.6	0.3	4 x 10^3
10 Flashes (5 J/cm², 500 µs)	13	0.6	-0.2	7 x 10^2
20 Flashes (5 J/cm², 500 µs)	36	0.2	-0.5	2 x 10^3
Thermal annealing at 250 °C for 1 hour	38	0	-0.7	1 x 10^4

operating characteristics comparable to that of optimized In_2O_3 TFTs processed with 20 pulses. The results suggests that the ZnO layer does not benefit electron transport across the channel probably due to its low compositional and structural quality.[26] On the other hand, a significant enhancement of the electron mobility by a factor of ~3 is achieved by treating the devices with 10 pulses. The latter leads to a 0.5 V shift of the V_{ON} towards more negative voltage,

indicative of the presence of a higher concentration of free electrons. The V_{TH} on the other hand remains unchanged due to the shallow slope of the transfer characteristic in the subthreshold regime which might indicate the presence of electron trap states in the bulk of the active area and/or at the interface with the gate dielectric.[27,28] Increasing the number of pulses to 20 results to a significant increase in the electron mobility to a value of ~36 cm^2/Vs accompanied by shifts in V_{ON} and V_{TH} towards negative voltages, both denoting a higher concentration of mobile electrons. We attribute this to the transfer of electrons from the conduction band (CB) of ZnO to that of the In_2O_3 driven by the significant difference in their work functions and CB energies.[10,18,19] Also hysteresis effects with a counter clockwise direction is also visible which could either originate from charge trapping/detrapping or ion migration in the gate dielectric.[29] Similar characteristics have been previously reported for metal oxide TFTs based on ZrO_X as well as Ta- or Hf-based dielectrics.[30] In particular, and relevant to this work, is the previous reports on oxide TFTs based on multilayer dielectrics composed of AlO_X and ZrO_X which have also shown to suffer from increased hysteresis, possibly indicating intrinsic instability of the dielectric system.[31] Thus we are confident that the device performance can be improved by switching to a gate dielectric that is less susceptible to hysteresis effects. In spite of this the resulting In_2O_3/ZnO TFTs show appreciable switching behaviour with an on/off channel current ratio of ~10^3. The corresponding output characteristics for the In_2O_3/ZnO heterostructure TFT is shown in **Fig. 2(b)**. Importantly, the overall performance of the photonically processed In_2O_3/ZnO TFTs is almost identical to that of the control In_2O_3/ZnO devices prepared via thermal annealing at 250 °C for 1 h (see **Table 2** and ESI,† **Fig. S7(c)**). Our results highlight the applicability of the photonic processing method for the growth of complex multilayer metal oxide structures in a facile and rapid manner.

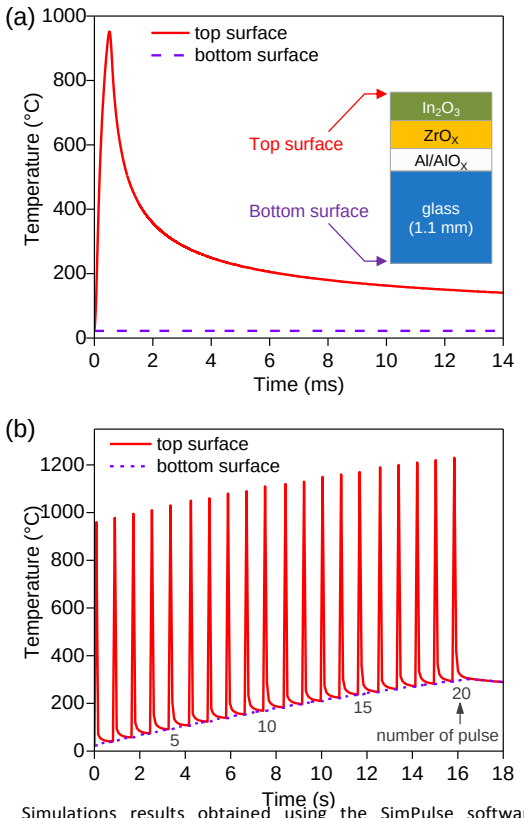

Fig. 3 Simulations results obtained using the SimPulse software of the temperature (°C) at the top and at the bottom of the In_2O_3 TFT fabricated on 1.1 mm-thick glass substrate after exposure to (a) a single xenon light pulse, and (b) 20 xenon light pulses at a fire rate of 1.2 Hz. The pulse duration energy density per pulse used were 5 J/cm² and 500 µs, respectively. Inset in (a) shows the schematic of the layered stack considered in the simulations.

Post-processing of sequentially deposited multilayer structures (enabled via intermittent soft-baking steps) using a single photonic treatment step resulted in reduced transistor performances most likely due to interdiffusion of the precursor materials. Although understanding the reason for the observed performance degradation is beyond the scope of this work, such knowledge may be key for reducing the complexity of the manufacturing process further.

To understand the temperature evolution across the different layers during optical pulsing, the thermal gradient in the In_2O_3 transistor structure shown in the inset of **Fig. 3** was simulated using the SimPulse software tool. This is a machine integrated thin film stack thermal modelling program that accounts for the system settings, the electrical performance, and optical efficiencies of the flash lamp system and combines that with an interactive thin-film stack thermal modeller to ultimately output the thermal response of the materials stack to that particular pulse sequence emitted by the tool. Typically, SimPulse is run in volumetric mode in which the Lambert–Beer law is used to model the absorption of the light as a function of depth in order to calculate the temperatures within the layers during and after the pulse sequence. A detailed explanation of the numerical model used is given elsewhere.[21,32]

Results of the simulation suggest that following a single xenon light pulse the temperature on the top surface of the stuck (In_2O_3/air interface) increases up to ~1000 °C whereas the backside of the substrate remains close to room temperature.

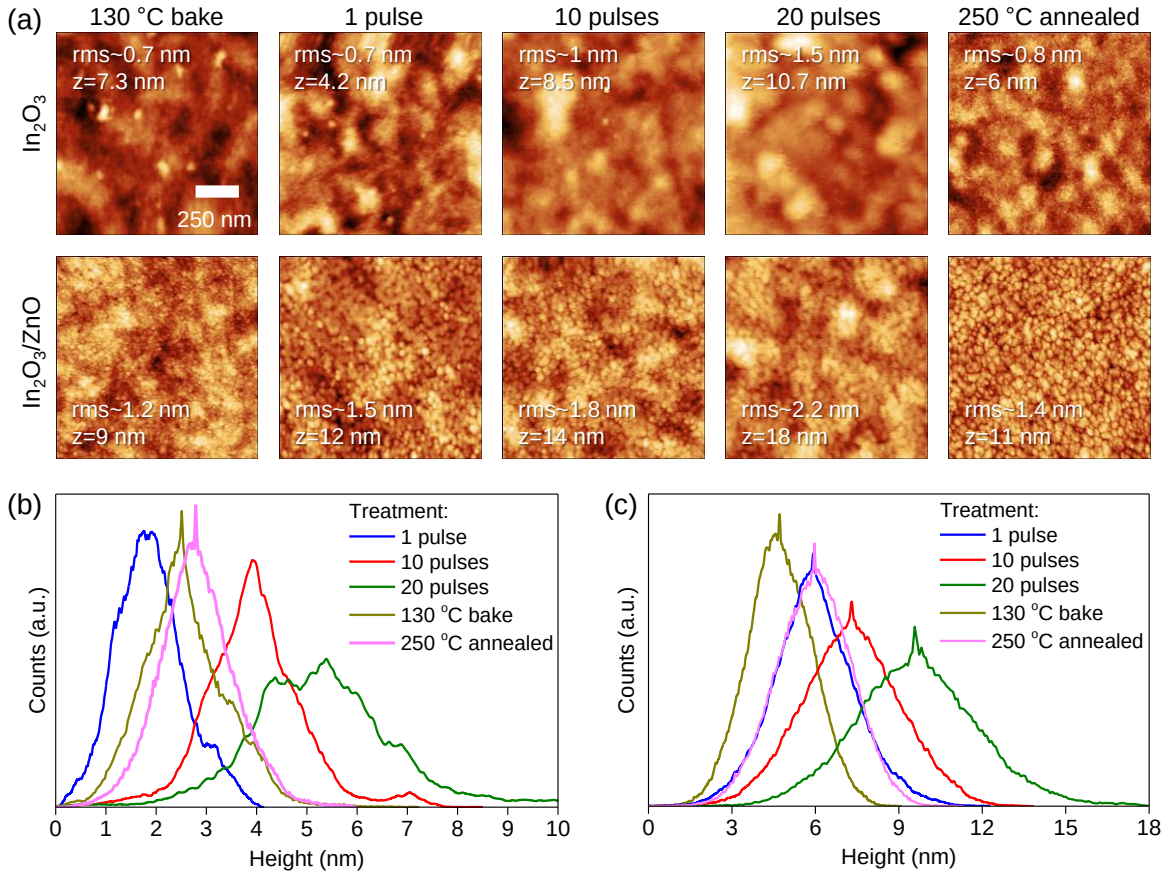

Fig. 4 (a) AFM surface topography images of In_2O_3 and In_2O_3/ZnO structures (deposited onto glass/Al/AlO_X/ZrO_X structures) subjected to: low-temperature thermal annealing (bake), photonic treatment using varying number of pulses and conventional thermal annealing at 250 °C. Corresponding height distributions for (b) In_2O_3 and (c) In_2O_3/ZnO.

Next, the top surface temperature reduces to <200 °C within only ~6 ms. Subjecting the device to 20 pulses results in a further increase of the surface temperature to >1200 °C. However, due to appreciable thermal conduction the temperature on the backside increases as well to ~300 °C followed by a drop to <200 °C within a few seconds. This characteristic back side temperature increase could in principle be reduced to significantly lower values through the use of substrate materials with lower thermal conductivity (e.g. plastics or paper).

The overall duration of the photonic processing involving 20 light pulses is only 16 s highlighting the rapid nature of the proposed method. Simulations of the temperature evolution in the In_2O_3/ZnO heterostructure device showed similar results with negligible temperature differences of ~4% compared to single layer In_2O_3 devices due to the presence of the additional ZnO layer.

The surface morphologies of the softly-baked, photonically treated and thermally annealed In_2O_3 and In_2O_3/ZnO structures were further analysed by AFM (**Fig. 4**). Softly-baked (130 °C) In_2O_3 precursor layers deposited onto Al/AlO_X/ZrO_X exhibit smooth surface characteristics with rms roughness of 0.7 nm. Subjecting these samples to a single xenon light pulse results to no significant change in the surface roughness. However, increasing the number of pulses to 10 and 20 is found to increase the surface rms roughness to ~1 and 1.5 nm, respectively. On the contrary, single layers of In_2O_3 that have been thermally annealed at 250 °C for 1 h show almost no change in the surface roughness. These differences can better be seen in the histograms of **Fig. 4b** where the 20 flashes sample exhibit the highest surface roughness manifested as a wider distribution of ~10 nm.

A similar trend is observed for the photonically cured ZnO layers deposited onto photonically treated In_2O_3 layers. By increasing the number of pulses the surface rms roughness of the ZnO layer increases manifested as a broadening and shift of the height distribution towards higher values (**Fig. 4c**). On the other hand, thermally annealed In_2O_3/ZnO heterostructures exhibited significantly smoother surfaces than equivalent samples subjected to 20 pulses. This is most likely due to the extremely smooth surface of the underlying In_2O_3 layer that acts as a planarization layer for ZnO. In general, photonically cured metal oxide films show a higher surface roughness than thermally annealed ones. We believe this is due to the rapid introduction of thermal energy which limits re-crystallisation within the converting layer. In contrast, use of long thermal annealing times allows self-diffusion of the metal oxide during conversion leading to a smoother layer surfaces.

X-ray photoelectron spectroscopy (XPS) was used to monitor changes in the surface chemistry of the photonically treated layers and compare them against those of thermally annealed samples (control) **(Fig. 5)**. Devices based on In_2O_3

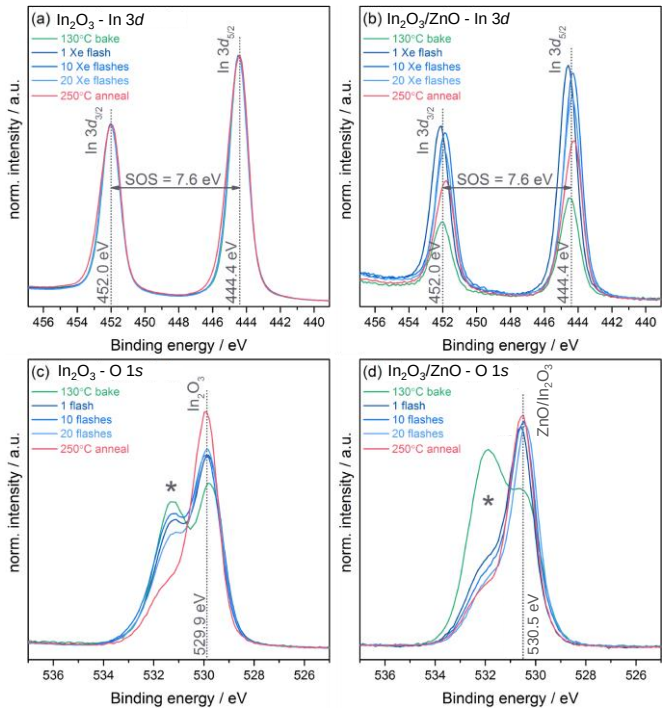

Fig. 5 In 3*d* and O 1*s* core level XPS spectra for (a) and (c) In_2O_3 layer, and (b) and (d) In_2O_3/ZnO heterostructure samples prepared using different methods, including photonic treatment and thermal annealing. A higher binding energy shoulder observed on the O 1*s* spectra is marked with an asterisk.

show typical In 3*d* core levels with an In $3d_{5/2}$ peak position of 444.4 eV and a spin-orbit-split (SOS) of 7.6 eV.[33,34] For In_2O_3/ZnO heterostructure devices both Zn 2*p* and $L_3M_{4,5}M_{4,5}$ show binding energy (BE) positions and structural features typical for ZnO (see ESI,† **Fig. S10**).[34,35] Although In_2O_3 is expected to be covered by a conformal layer of ZnO and XPS is highly surface sensitive (with an inelastic mean free path (IMFP) of 2.0 nm in ZnO as calculated using the TPP-2M method incorporated in the QUASES software package)[36], In is detected in all samples. We attribute this to a combination of material interdiffusion, surface roughness and other surface imperfections such as pinholes.[10] A clear difference in In 3*d* intensities (normalised to the Zn $2p_{3/2}$ intensity) is found between the different samples with the photonically treated systems exhibiting a higher percentage of In as compared to the thermally annealed layers. Relative atomic Zn:In ratios were obtained from peak fit analysis to the In $3d_{5/2}$ and Zn $2p_{3/2}$ lines and are summarised in **Table 3**. Small changes in the indium BE are found which have been previously observed on bilayer In_2O_3/ZnO samples and are attributed to a change in the direct chemical environment of In, e.g. differences in oxygen coordination of In caused by varying concentration of oxygen vacancies.[10]

Table 3 Relative atomic ratios from peak fit analysis of XPS core level spectra in In_2O_3 and In_2O_3/ZnO structures.

Sample	O_{In2O3}:O* (In_2O_3)	$O_{ZnO/In2O3}$:O* In_2O_3/ZnO)	Zn:In (In_2O_3/ZnO)
130 °C soft-bake	46:54	37:63	98.7:1.3
1 Pulse	51:49	65:35	97.0:3.0
10 Pulse	48:52	70:30	97.1:2.9
20 Pulse	54:46	70:30	97.4:2.6
250 °C annealing	69:31	82:18	97.8:2.2

The O 1*s* spectra for both single layer and bilayer samples show two resolved peaks. The main oxide peak is at 529.9 eV in the single layer films, which corresponds to In_2O_3, and at 530.5 eV in the heterostructure films corresponding to ZnO with some contribution from In_2O_3. The higher BE peak (marked with an asterisk in **Fig. 5**) can be assigned to hydroxide groups, with

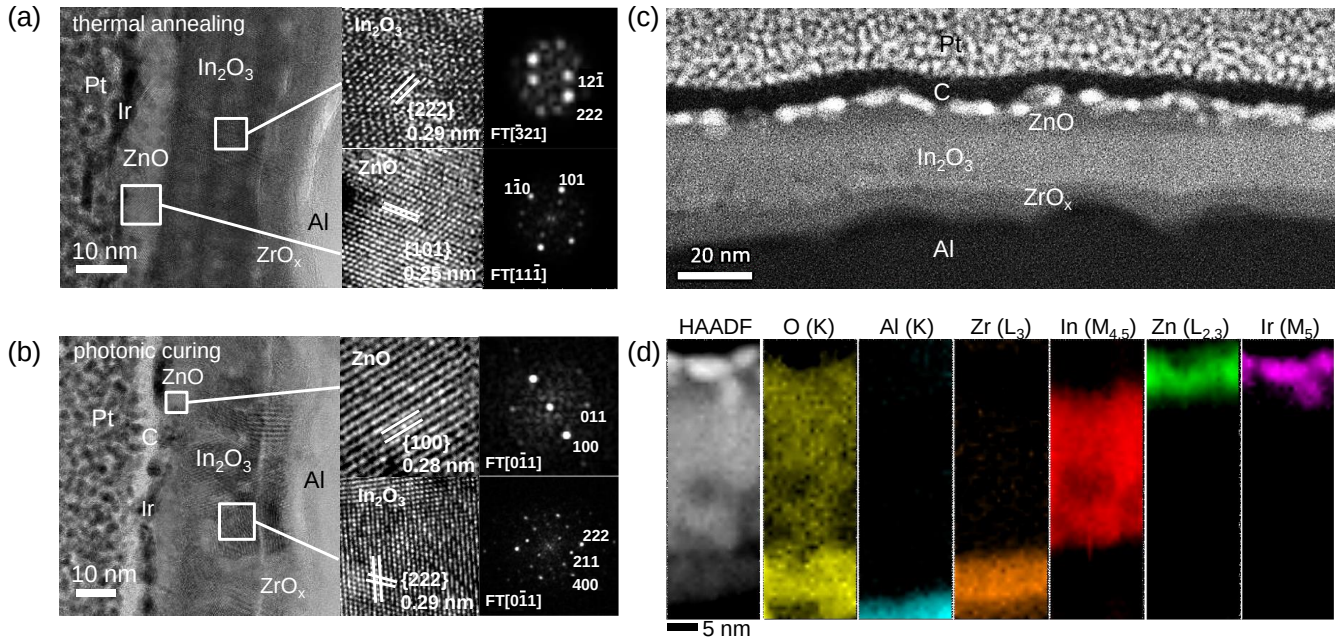

Fig. 6 High-resolution transmission electron microscope (HRTEM) cross-section images of In_2O_3/ZnO heterostructures treated by: (a) thermal annealing at 250 °C and (b) photonic curing using 20 xenon flash pulses of energy densities of 5 J/cm² and pulse durations of 500 µs at a fire rate of 1.2 Hz for each layer. (c) Scanning transmission electron microscopy (STEM) of photonically cured In_2O_3/ZnO heterostructures, and (d) electron energy loss spectroscopy (EELS) mapping.

some contribution from oxidised C and N species (see ESI,† **Fig. S11** for the C and N 1s core level). Its intensity clearly reduces relative to the main oxide peak after the xenon flash annealing compared to the 130 °C baked samples, with the 20 flash samples having the highest oxide intensity for both sample groups. This reduction is linked to a better conversion of hydroxide-related precursor species into metal oxides leading to an increased semiconductor quality. It should be emphasized here that the hydroxide contribution in the In_2O_3/ZnO heterostructure is significantly reduced as compared to the single layer In_2O_3 sample following photonic treatment. Since the IMFP is approximately 2 nm, the result is attributed to the properties of the ZnO layer present at the top of the heterostructure. The lower hydroxide signal in ZnO is attributed to the lower conversion temperature of the precursor formulation employed (≈100 °C) as compared to that for In_2O_3 (≥200 °C). Indeed, our previous investigations have shown that devices based on ZnO layers prepared using the same method can reach mobilities of ≈1 cm^2/Vs when annealed at 100 °C, whereas a temperature of ≈200 °C is required for achieving comparable performance in In_2O_3 transistors.[10,26] The higher precursor conversion rate in photonically and thermally annealed samples is further confirmed by an overall reduction of N species in the N 1*s* core level. **Table S2** summarises the In/Zn to N ratio for all thin films. The bilayer samples overall have a lower residual N amount after all treatments, most likely due to a different conversion rate of the Zn versus the In precursor.

The microstructure of photonically and thermally converted In_2O_3/ZnO heterostructures was further examined by cross-sectional high-resolution transmission electron microscopy (HRTEM). As shown in **Fig. 6(a)** the bottom In_2O_3 layer of thermally annealed (250 °C) devices features a high microstructural order with a lattice spacing of 0.29 nm corresponding to the (222) plane. This was further verified by Fast Fourier Transform (FFT) calculations as well as the presence of an additional orientation along the (12 $\bar{1}$) plane. The top ZnO layer showed a similar polycrystalline character with two prominent spacings corresponding to the (101) and (1 $\bar{1}$ 0) planes. In addition, the analysis of the HRTEM image yields layer thicknesses for the ZrO_X, In_2O_3 and ZnO in the range of 6-7 nm, 15-17 nm and 4-5 nm, respectively. Similar thickness values were measured for the photonically annealed heterostructure shown in **Fig. 6(b)**. However, here, the bottom In_2O_3 layer appears to be more inhomogeneous consisting of many randomly orientated nanocrystals. Nevertheless, the lattice spacing remains the same (i.e. 0.29 nm corresponding to the (222) plane) and is found not to be influenced by the subsequent photonic treatment of the top ZnO layer. The latter layer also shows slight differences in the crystal structure compared to thermally annealed ZnO layers with the prominent lattice spacing of 0.28 nm corresponding to the (100) plane.

The elemental composition of the photonically cured In_2O_3/ZnO heterojunction was also studied using scanning transmission electron microscopy (STEM) and electron energy loss spectroscopy (EELS). As can be seen in the STEM image in **Fig. 6(c)** the layers of ZrO_X, In_2O_3 and ZnO are clearly resolvable as distinct separate layers which is further verified by the EELS analysis shown in **Fig. 6(d)**. These data indicate the presence of chemically sharp interfaces between the ZrO_X, In_2O_3 and ZnO layers with no signs of significant interdiffusion or alloying of the respective layers as a result of the photonic treatment. The presence of such high quality heterointerfaces support the exceptional performance achieved in the photonically treated In_2O_3/ZnO heterojunction TFTs shown in **Fig. 2**, while at the same time highlights the applicability of the method for the rapid development of simple as well as complex multi-layer metal oxide structures and devices.

Conclusions

In conclusion, we successfully employed a photonic-based process for the rapid chemical conversion of different solution-processed metal oxide precursors to high quality single layer In_2O_3 as well as In_2O_3/ZnO heterostructures on glass substrates. These carefully engineered semiconducting systems were subsequently employed as the electron-transporting layers in low-operating voltage (<2 V) TFTs where electron mobility values of up to 36 cm^2/Vs were obtained. This level of performance is comparable to that achieved in control transistors fabricated via conventional thermal annealing at 250 °C for 1 h but at a fraction of the processing time. Our results demonstrate the tremendous potential of this alternative approach for the rapid processing of metal oxide electronics over large-area substrates.

Acknowledgements

The authors would like to thank Kurt A. Schroder and John Passiak from Novacentrix for the access to SimPulse in order to carry out all relevant simulations in this study. This work was funded by the People Programme (Marie Curie Actions) of the European Union's Framework Programme Horizon2020: "Flexible Complementary Hybrid Integrated Circuits" (FlexCHIC), grant agreement no. 658563.

References

1 X. Yu, T. J. Marks and A. Facchetti, *Nature Materials*, 2016, **15**, 383.
2 E. Fortunato, P. Barquinha and R. Martins, *Adv. Mater.*, 2012, **24**, 2945.
3 L. Petti, N. Münzenrieder, C. Vogt, H. Faber, L. Büthe, G. Cantarella, F. Bottacchi, T. D. Anthopoulos and G. Tröster, *Appl. Phys. Rev.*, 2016, **3**, 021303.
4 J.-P. Jolivet, M. Henry and J. Livage, *Metal oxide chemistry and synthesis: from solution to solid state*. Wiley-Blackwell, 2000.
5 S. Inoue, T. T. Phan, T. Hori, H. Koyama and T. Shimoda, *Phys. Status Solidi A*, 2015, **212**, 2133.
6 Y. S. Rim, H. Chen, B. Zhu, S.-H. Bae, S. Zhu, P. J. Li, I. C. Wang and Y. Yang, *Adv. Mater. Interfaces*, 2017, 1700020.
7 K. Myny, M. Rockelé, A. Chasin, D.-V. Pham, J. Steiger, S. Botnaras, D. Weber, B. Herold, J. Ficker, B. van der Putten, G. H. Gelinck, J. Genoe, W. Dehane and P. Heremans, *IEEE Trans. Electron Dev.*, 2014, **61**, 2387.

8 C.-H. Choi, L.-Y. Lin, C.-C. Cheng and C.-H. Chang, *ECS J. Solid State Sci. Technol.,* 2015, **4**, P3044.
9 G. Adamopoulos, S. Thomas, P. H. Woebkenberg, D. D. C. Bradley, M. A. McLachlan and T. D. Anthopoulos, *Adv. Mater.*, 2011, **23**, 1894.
10 K. Tetzner, I. Isakov, A. Regoutz, D. J. Payne and T. D. Anthopoulos, *J. Mater. Chem. C*, 2017, **5**, 59.
11 S. Dellis, I. Isakov, N. Kalfagiannis, K. Tetzner, T. D. Anthopoulos and D. C. Koutsogeorgis, *J. Mater. Chem. C*, 2017, **5**, 3673.
12 C.-M. Kang, H. Kim, Y.-W. Oh, K.-H. Baek and L.-M. Do, *IEEE Electron Dev. Lett.*, 2016, **37**, 595.
13 D. W. Kim, J. Park, J. Hwang, H. D. Kim, J. H. Ryu, K. B. Lee, K. H. Baek, L.-M. Do and J. S. Choi, *Electron. Mater. Lett.*, 2015, **11**, 82.
14 S. C. Park, D. Kim, H. Shin, D. K. Lee, X. Zhang, J. Park and J. S. Choi, *J. Inf. Disp.*, 2016, **17**, 1.
15 T.-H. Yoo, S.-J. Kwon, H.-S. Kim, J.-M. Hong, J. A. Lim and Y.-W. Song, *RSC Adv.*, 2014, **4**, 19375.
16 W. H. Lee, S. J. Lee, J. A. Lim and J. H. Cho, *RSC Adv.*, 2015, **5**, 78655.
17 M. Smith, R. A. McMahon, M. Voelskow and W. Skorupa, *J. Appl. Phys.*, 2004, **96**, 4843.
18 Y.-H. Lin, H. Faber, J. G. Labram, E. Stratakis, L. Sygellou, E. Kymakis, N. A. Hastas, R. Li, K. Zhao, A. Amassian, N. D. Treat, M. McLachlan and T. D. Anthopoulos, *Adv. Sci.*, 2015, **2**, 2198.
19 J. G. Labram, Y.-H. Lin and T. D. Anthopoulos, *Small*, 2015, **11**, 1613.
20 Y. M. Park, A. Desai and A. Salleo, *Chem. Mater.*, 2013, **25**, 2571.
21 M. J. Guillot, S. C. Cool, *Int J Numer Method H*, 2015, **25**, 950.
22 K. A. Schroder, *Nanotechnology 2011: Electronics, Devices, Fabrication, MEMS, Fluidics and Computational,* 2011, **2**, 220.
23 K. Tetzner, K. A. Schroder, K. Bock, *Ceram. Int.*, 2014, **40**, 15753.
24 M. Bass, C. DeCusatis, J. Enoch, V. Lakshminarayanan, G. Li, C. Macdonald, V. Mahajan, E. Van Stryland, *Handbook of Optics, Third Edition Volume II: Design, Fabrication and Testing, Sources and Detectors, Radiometry and Photometry*, third ed., McGraw-Hill Inc, New York, NY, USA, 2010.
25 J. Socratous, K. K. Banger, Y. Vaynzof, A. Sadhanala, A. D. Brown, A. Sepe, U. Steiner and H. Sirringhaus, *Adv. Funct. Mater.*, 2015, **25**, 1873.
26 Y.-H. Lin, H. Faber, K. Zhao, Q. Wang, A. Amassian, M. McLachlan and T. D. Anthopoulos, *Adv. Mater.*, 2013, **25**, 4340.
27 M. Oertel, T. Balster and V. Wagner, *J. Appl. Phys.*, 2013, **114**, 234502.
28 S. M. Jin, N.-I. Cho, E.-J. Yun and H. G. Nam, *Thin Solid Films*, 2013, **527**, 334.
29 W. Xu, M. Dai, L. Liang, Z. Liu, X. Sun, Q. Wan and H. Cao, *J. Phys. D: Appl. Phys.*, 2012, **45**, 205103.
30 J. W. Jin, A. Nathan, P. Barquinha, L. Pereira, E. Fortunato, R. Martins and B. Cobb, *AIP Advances*, 2016, **6**, 85321.
31 H. Kim, Y.-J. Kwack, E.-J. Yun and W.-S. Choi, *Sci. Rep.*, 2016, **6**, 33576.
32 M. J. Guillot, S. C. McCool and K. A. Schroder, *ASME International Mechanical Engineering Congress and Exposition, Volume 7: Fluids and Heat Transfer, Parts A, B, C, and D,* 2012, 19-27.
33 C. Körber, V. Krishnakumar, A. Klein, G. Panaccione, P. Torelli, A. Walsh, J. L. F. Da Silva, S.-H. Wei, R. G. Egdell and D. J. Payne, *Phys. Rev. B: Condens. Matter Mater. Phys.*, 2010, **81**, 165207.
34 R. Henríquez, E. Muñoz, E. A. Dalchiele, R. E. Marotti, F. Martín, D. Leinen, J. R. Ramos-Barrado and H. Gómez, *Phys. Status Solidi A*, 2013, **210**, 297.
35 V. Dimitrov and T. Komatsu, *J. Solid State Chem.*, 2002, **163**, 100.
36 S. Tanuma, C. J. Powell and D. R. Penn, *Surf. Interface Anal.*, 1994, **21**, 165.